McWilliams et al., http://www.jcb.org/cgi/content/full/jcb.201603039/DC1

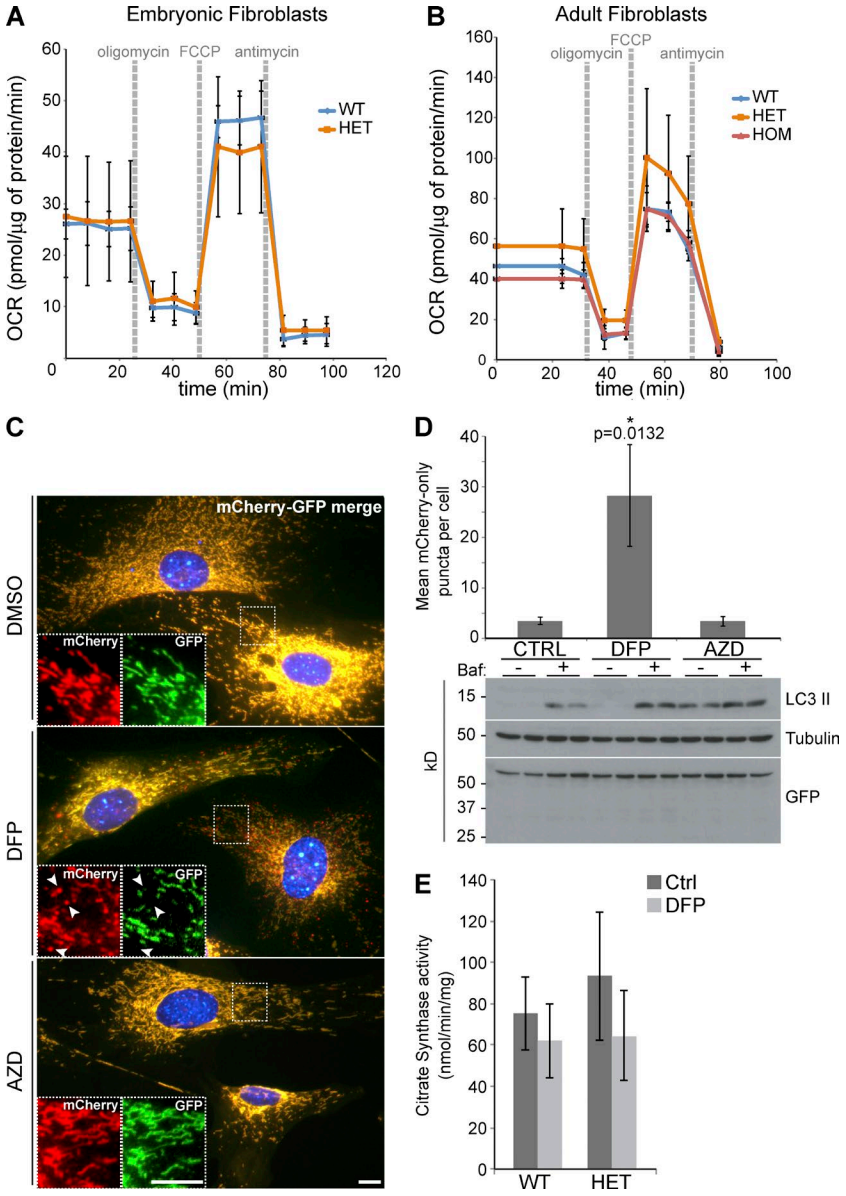

Figure S1. **In vitro characterization of *mito*-QC.** (A and B) Analysis of mitochondrial oxygen consumption rate (OCR) in MEFs (A) and adult lung fibroblasts (B) isolated from *mito*-QC mice. 1 µM oligomycin A, 1 µM FCCP, and 10 µM antimycin A were injected at the indicated times to determine the proportion of oxygen consumption caused by ATP turnover, maximal rate of respiration, and amount of proton leak, respectively. WT, wild-type cells; HET, heterozygous *mito*-QC cells; HOM, homozygous *mito*-QC cells. Error bars in A and B represent standard deviation with cells from a single mouse per genotype, with four (A) and three (B) replicates. (C) Assessment of stimulus-induced mitophagy in cultured primary MEFs. MEFs were treated with 1 mM deferiprone (DFP) or vehicle alone (DMSO) for 24 h as well as 1 µM mTOR inhibitor AZD8055 (AZD) before fixing and visualizing mitochondrial reporter by fluorescence microscopy. DAPI is shown in blue. Arrowheads highlight mCherry-positive, GFP-negative puncta. Bars, 10 µm. (D) Quantitation of data presented in C, from three independent experiments showing mean mCherry-only puncta per cell; error bars represent standard error, and significance was determined by one-way analysis of variance and Tukey's honest significant difference test. In parallel, cells were also treated as in C with/without 50 nM bafilomycin A1 for the final 2 h to observe autophagic flux. Cells were lysed and subjected to SDS-PAGE, transferred to polyvinylidene fluoride, and blotted with the indicated antibodies. All conditions were loaded in duplicate. (E) Citrate synthase activity in primary MEFs treated with/without 1 mM DFP for 24 h. Results represent mean activities from MEFs isolated from three different wild-type (WT) or heterozygous (HET) embryos. Error bars represent standard error.

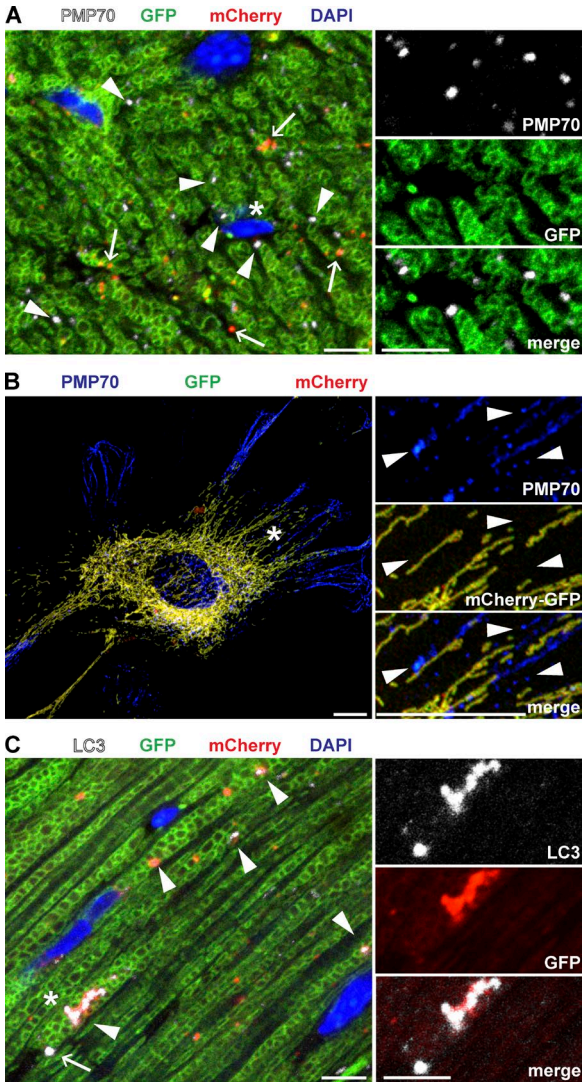

Figure S2. ***mito*-QC indicates delivery of mitochondrial to autolysosomes and staining in general is distinct from peroxisomal staining.** (A) Representative image of *mito*-QC heart tissue section immunolabeled with antibodies to the peroxisomal marker PMP70. Bars, 5 µm. Arrowheads indicate examples of distinct PMP70-only staining and arrows indicate mCherry-only structures. Asterisk marks the area magnified in the panels to left, highlighting the distinct, but closely associated, peroxisomal (PMP70) and mitochondrial (GFP) staining. (B) Primary *mito*-QC heterozygous MEFs fixed and stained with anti-PMP70. Bars, 10 µm. Asterisk marks the area magnified in the panels to left, and arrowheads highlight that PMP70 staining is distinct from the mCherry-GFP signal. (C) Representative image of *mito*-QC heart tissue section immunolabeled with antibodies to the autophagosomal/autolysosomal marker LC3b. Bars, 5 µm. Arrowheads indicate examples of LC3/mCherry-only (GFP-negative) colocalization (autolysosomes), and arrow indicates LC3-only structure (autophagosome). Asterisk marks the area magnified in the panels to left, highlighting colocalization between LC3 and mCherry-only puncta.

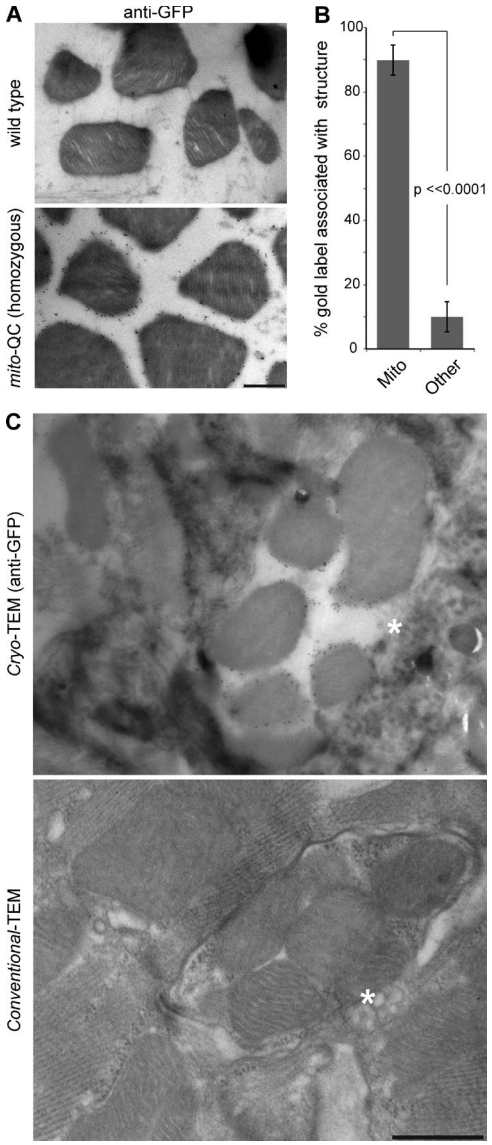

Figure S3. **GFP-immunolabeling is highly specific for mitochondria as visualized by EM.** (A) Representative mitochondrial cryo-electron micrographs of heart sections from wild-type (top) or homozygous *mito*-QC mice (bottom) labeled with anti-GFP gold-conjugated antibodies. Bar, 500 nm. Staining was highly specific with a mitochondrial labeling density of 13.6 gold particles per square micrometer for *mito*-QC, compared with 0.4 per μm^2 for wild type mice. (B) Quantitation of gold particle localization in homozygous *mito*-QC heart. Values indicate the percentage of gold particles associated with mitochondria as opposed to nonmitochondrial staining. A total of 2,615 particles were counted from 24 individual images. Error bars represent standard deviation, and significance was determined using an unpaired, two-tailed Student's *t* test. (C) Example cryotransmission electron micrograph (TEM) of GFP-gold labeled mitochondria in an autophagosomal-like structure (top panel marked with asterisk) in a *mito*-QC heart. In the bottom panel, the asterisk indicates a similar mitophagic structure also in a *mito*-QC heart, as visualized using conventional resin transmission EM, which highlights the double lipid bilayer of the surrounding autophagic membrane. Bar, 500 nm.

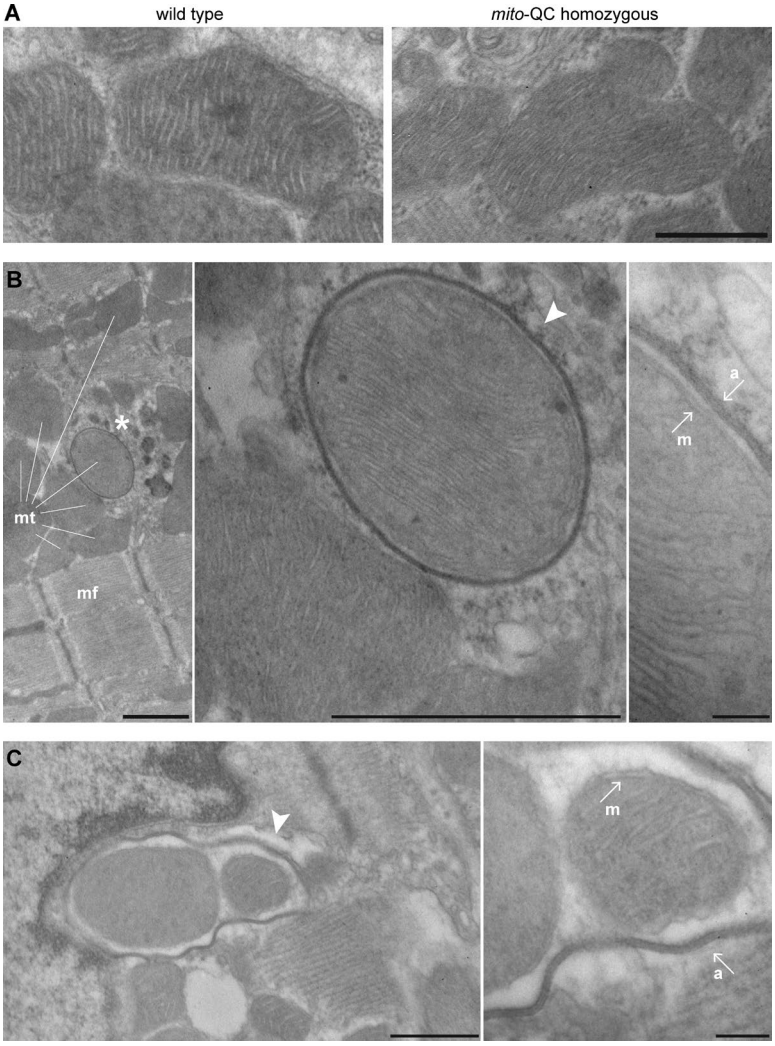

Figure S4. **Comparative assessment of cardiac mitochondrial morphology and mitophagy in wild-type and reporter mice.** (A) Electron micrograph highlighting the identical mitochondrial structure in wild type (left panel) and homozygous *mito*-QC (right) heart ventricle. Bar, 500 nm. (B, left) Representative micrograph from *mito*-QC heart ventricle indicating mitochondria (mt) and adjacent myofibril (mf). Asterisk marks a mitophagosome that is shown magnified in the middle panel of B. Arrowhead indicates area further magnified in the right panel. Autophagosome double lipid bilayer (a) and mitochondrial outer double lipid bilayer (m) are indicated. Bars: (B, left and middle) 1 µm; (B, right) 100 nm. (C) Example of mitophagy from wild-type mouse heart ventricle, with mitophagosome highlighted by arrowhead, which is further magnified in the right panel. Autophagosome double lipid bilayer (a) and mitochondrial outer double lipid bilayer (m) are indicated. Bars: (C, left) 500 nm; (C, right) 100 nm.

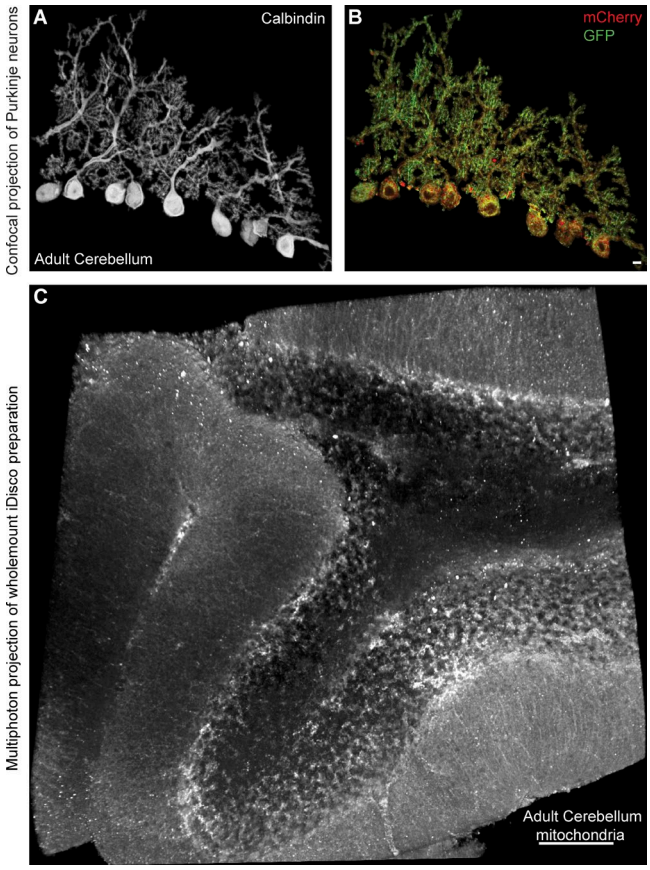

Figure S5. ***mito*-QC is compatible with contemporary techniques in histochemistry and whole-tissue imaging.** (A and B) Volocity-generated digital mask of calbindin-positive Purkinje neurons in the adult cerebellum, obtained from a conventional confocal Z-stack of an immunolabeled cryosection. For clarity, calbindin staining is depicted in A and *mito*-QC signals are depicted in B. Bar, 5 µm. (C) Multiphoton projection of mitochondria within intact, unlabeled iDISCO preparations of adult cerebellum. Bar, 100 µm.

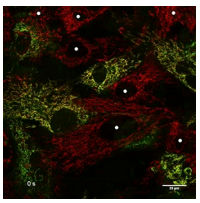

Video 1. **Mitochondrial dynamics in wild-type and mito-QC MEFs.** Mixed cultures of wild-type and heterozygous *mito*-QC MEFs were labeled with MitoTracker far red. Live-cell imaging shows GFP-positive *mito*-QC cells, and far red (red)–positive wild-type and *mito*-QC cells. White dots mark wild-type cells (GFP negative). Bar, 20 µm.

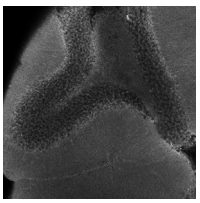

Video 2. **Mitochondrial architecture in the cerebellum.** Video showing 2D Z-stack of the mCherry signal indicating the total mitochondrial pool in an intact lobe of adult *mito*-QC cerebellum. Tissue was processed using iDISCO for two-photon microscopy as indicated in Materials and methods. Scale indicated by width of frame (708 µm).

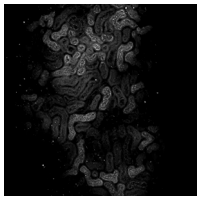

Video 3. **Mitochondria and mitophagy in the renal cortex.** Video showing 2D Z-stack of the mCherry signal indicating the total mitochondrial pool in an intact adult *mito*-QC kidney. Video shows lateral-medial transition from the renal cortex to the medulla. Tissue was processed using iDISCO for two-photon microscopy as indicated in Materials and methods. Note bright punctate staining (mitophagy) in the apical (luminal) side of certain tubular cells. Scale indicated by width of frame (708 µm).